engineering proceedings

MDPI

Proceeding Paper

Dynamic Modeling Analysis of a Doubly-Fed Induction Generator-Based Wind Energy System †

Sardorjon Samiev [1,*], Shokhabbos Doliev [1], Javlonbek Khamraev [1], Golibjon Makhmatqulov [2] and Khurshid Yusupov [1]

[1] Department of Information Technologies in Industry and Tourism, Shahrisabz Faculty of Food Engineering, Karshi State Technical University, Shahrisabz 181306, Uzbekistan; shokhabbos9109@gmail.com (S.D.); hamrayevjavlonbek11@gmail.com (J.K.); yusupovxurshid1995@gmail.com (K.Y.)

[2] Department of Economics, Faculty of Pedagogy, University of Economics and Pedagogy, Karshi 180100, Uzbekistan; golibmaxmatqulov@gmail.com

* Correspondence: sardorjonsamiyev95@gmail.com; Tel.: +998-973990925

† Presented at the The 1st International Online Conference on Inventions, Energy Security and Sustainable Development, 25–26 June 2026; Available online: https://sciforum.net/event/IOCIV2026.

Abstract

The increasing integration of wind energy into modern power systems introduces significant challenges in maintaining frequency stability and power quality due to the stochastic nature of wind speed, particularly in microgrid environments. This study focuses on the modeling and control of a wind energy conversion system based on a Doubly Fed Induction Generator (DFIG) operating in conjunction with an external power supply system. A comprehensive simulation model of the wind energy system was developed in MATLAB (R2023b), incorporating both the wind turbine and power converter subsystems. The control strategy is based on stator flux-oriented vector control, which enables independent regulation of active and reactive power, combined with space vector pulse-width modulation (SVPWM) to improve the performance of the power electronic converters. The system employs a dual-converter structure, where the rotor-side converter ensures bidirectional power flow and the grid-side converter maintains the DC-link voltage. The simulation results demonstrate that the proposed control system ensures fast dynamic response and stable operation under variable wind conditions. In particular, the stator current reaches a steady state within 0.01 s, satisfying the specified technical requirement for transient performance. Additionally, the DC-link voltage is effectively stabilized at approximately 700 V, ensuring reliable operation of the converter system. The use of SVPWM contributes to improved switching performance and efficient synthesis of voltage vectors, enhancing overall system stability. The developed model also confirms the stable operation of the wind energy system within a microgrid, ensuring coordinated interaction between system components under fluctuating wind conditions. Compared to conventional approaches, the applied vector control strategy provides effective decoupling of power components and improved dynamic characteristics for the system. The results obtained validate the effectiveness of the proposed modeling and control approach for small-scale wind energy systems and demonstrate its applicability for improving the stability and performance of renewable energy integration in modern power systems.

Keywords: DFIG; wind energy; vector control; frequency stability; MATLAB/Simulink; renewable energy; dynamic modeling

Check for updates

Academic Editor: Eugen Rusu

Published: 11 September 2026

Copyright: © 2026 by the authors. Licensee MDPI, Basel, Switzerland. This article is an open access article distributed under the terms and conditions of the Creative Commons Attribution (CC BY) license.

1. Introduction

Wind energy has become one of the most rapidly developing renewable energy sources, owing to its wide availability, environmental friendliness, and the decreasing cost of generation equipment [1–3]. As distributed generation increasingly penetrates conventional power networks, small-scale wind energy conversion systems are frequently combined with local loads and external supply systems to form microgrids [4], which are characterized by relatively low voltage levels, limited inertia, and high sensitivity to fluctuations introduced by renewable sources. Because wind speed varies continuously and unpredictably, the amplitude, frequency, and phase of the generated power fluctuate considerably more than in conventional synchronous generation, which makes frequency and voltage stability a central concern in the design of wind power conversion systems intended for grid-connected or microgrid operation [5].

Among the available wind turbine generator topologies, the Doubly Fed Induction Generator (DFIG) remains one of the most widely adopted solutions for variable-speed wind turbines rated from a few tens of kilowatts up to several megawatts [6,7]. In a DFIG-based system, the stator winding is directly connected to the grid at a constant frequency and voltage, while the rotor winding is fed through a back-to-back AC/DC/AC converter that only needs to handle a fraction (typically 25–30%) of the total generator power, since the converter only processes the slip power. This partial-scale power electronic interface gives the DFIG configuration a substantial cost advantage over full-scale converter topologies used with permanent-magnet direct-drive generators [8], while still allowing independent control of active and reactive power and operation across both sub-synchronous and super-synchronous speed ranges.

The control of a DFIG wind energy conversion system is conventionally divided into two coordinated tasks: control of the rotor-side converter (RSC), which regulates the electromagnetic torque and the active/reactive power exchanged with the grid through the stator, and control of the grid-side converter (GSC), which is primarily responsible for maintaining a stable DC-link voltage and ensuring a near-unity power factor on the grid side [9]. Vector control techniques based on stator-flux or stator-voltage orientation are commonly used to decouple the active and reactive power channels into independently controllable d- and q-axis current components [6,10], which significantly simplifies controller design and improves dynamic response. Space vector pulse-width modulation (SVPWM) is widely used to synthesize the converter switching pattern because of its superior DC-link utilization, lower harmonic distortion, and smoother torque output compared with conventional sinusoidal PWM [11].

Despite the maturity of DFIG control theory, the transient behavior of the system—particularly the settling time of the stator current and the dynamic stabilization of the DC-link voltage during start-up and wind-speed variation—remains an important practical design criterion, since fast and well-damped transients are required for reliable interconnection with an external power supply system and for compliance with grid-code requirements on fault ride-through and power quality [12]. Existing studies have addressed wind turbine aerodynamic modeling, DFIG electromechanical modeling, and converter control separately in many cases, while comprehensive system-level studies that simultaneously verify aerodynamic, electrical, and converter-level performance against an explicit transient-response specification are comparatively less common in the literature.

The objective of this study is to develop and verify, through MATLAB/Simulink simulation, a complete model of a small-scale wind energy conversion system based on a DFIG operating jointly with an external power supply system [13], in which the wind turbine aerodynamic model, the DFIG electromechanical model, and the dual-converter control system (RSC and GSC, both governed by stator-flux-oriented vector control and

https://doi.org/10.3390/engproc2026152010

SVPWM) are integrated into a single simulation framework. The specific technical requirement adopted for controller verification is that the stator current must reach a steady state within no more than 0.01 s following start-up, in addition to maintaining a stable DC-link voltage suitable for reliable converter operation. The remainder of the paper is organized as follows.

2. Materials and Methods

2.1. System Configuration and Study Object

The wind energy conversion system studied in this work consists of a horizontal-axis wind turbine, a two-stage gearbox, a DFIG, and a back-to-back AC/DC/AC power converter that connects the rotor circuit to the grid in parallel with the directly grid-connected stator circuit. The overall structure of the system is shown in Figure 1. The wind turbine captures the kinetic energy of the incoming airstream and converts it into mechanical torque on the low-speed shaft; the gearbox increases the rotor speed from the typical range of 10–30 rpm to the level required by the generator; the DFIG converts the mechanical power into electrical power, exporting part of it directly through the stator and exchanging the remaining slip power bidirectionally through the rotor-side and grid-side converters.

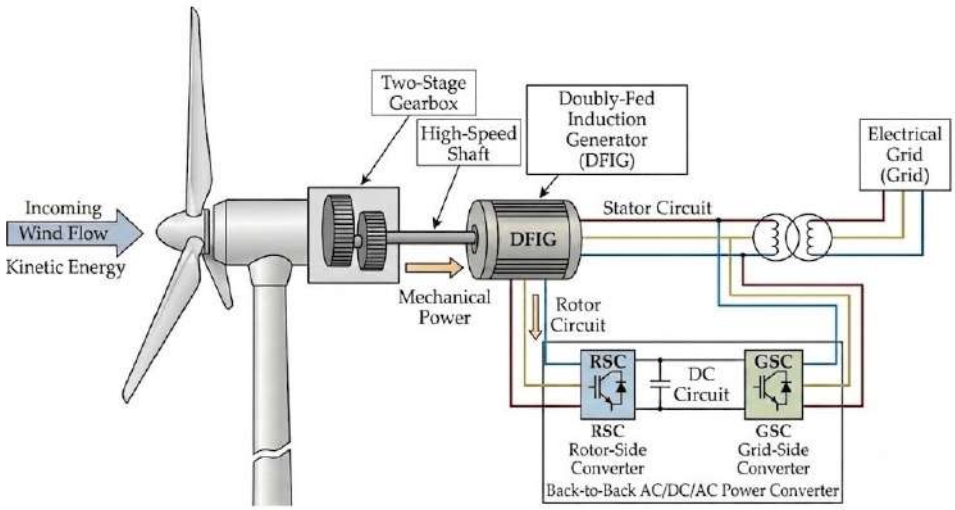


Figure 1. General structure of the DFIG wind energy conversion system and its rotor-side/grid-side control loops.

A horizontal-axis configuration was selected for the wind turbine rotor instead of a vertical-axis design. Although vertical-axis turbines offer wind-direction independence, lower installation height and reduced noise, their lower hub height, lower aerodynamic efficiency and higher relative manufacturing cost make horizontal-axis turbines preferable for the power and efficiency requirements adopted in this study; horizontal-axis turbines also achieve a higher power coefficient, simpler manufacturing, and better scalability for the modular structure required in a microgrid-connected installation.

2.2. Aerodynamic Model of the Wind Turbine

The mechanical power extracted from the wind by the turbine rotor is described by the standard aerodynamic power equation:

$$P_{wt} = \frac{1}{2}\rho\pi R^2 v^3 C_p(\lambda,\ \beta) \tag{1}$$

where ρ is the air density (taken as 1.205 kg/m^3 at 20 °C), πR^2 is the swept area of the rotor, v is the wind speed, and C_p is the power coefficient, which depends on the tip-speed ratio

λ and the blade pitch angle β. The tip-speed ratio is defined as $\lambda = \omega R/v$, where ω is the rotor angular speed and R is the rotor radius. The power coefficient is modeled by the widely used empirical expression [14]:

$$\begin{cases} C_p = 0.22\left(\frac{116}{\lambda_a} - 0.4\beta - 5\right)e^{\frac{-12.5}{\lambda_a}} \\ \lambda_a = \left(\frac{1}{\lambda + 0.08\beta} - \frac{0.035}{\beta^3 + 1}\right)^{-1} \end{cases} \quad (2)$$

The relationship between the power coefficient and the tip-speed ratio for several pitch angles, obtained from Equation (2), is presented in Figure 2. At zero pitch angle the curve reaches its maximum value $C_{p.max} \approx 0.43$ at the optimal tip-speed ratio $\lambda_{opt} \approx 9$, which defines the maximum power point operating locus that the turbine control system attempts to track as wind speed varies (Figure 3).

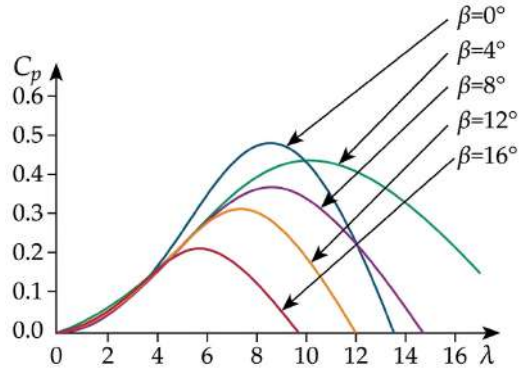


Figure 2. Power coefficient C_p as a function of the tip-speed ratio λ for pitch angles $\beta = 0 \ldots 16°$.

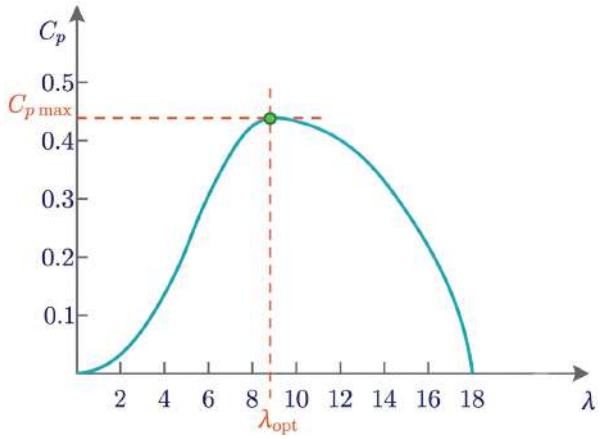


Figure 3. Characteristic curve of the wind rotor showing the maximum power coefficient at the optimal tip-speed ratio λ_{opt}.

Using Equation (1) and the target rated electrical output of 100 kW at the rated wind speed of 10 m/s, the minimum rotor radius was calculated from:

$$100 \cdot 10^3 = \frac{1}{2}(1.205)\pi R^2 (10)^3 (0.43) \quad (3)$$

which yields a minimum rotor radius of $R \approx 11.08$ m. This value was adopted for the simulated wind turbine model implemented in MATLAB/Simulink (Figure 4), in which wind speed and the generator rotor speed feedback are used as inputs, the tip-speed ratio and power coefficient are computed online, and the resulting mechanical torque T_m is supplied to the DFIG shaft, while the maximum power point tracking (MPPT) block

computes the reference torque and reference power required to keep the turbine operating near λ_{opt} [15].

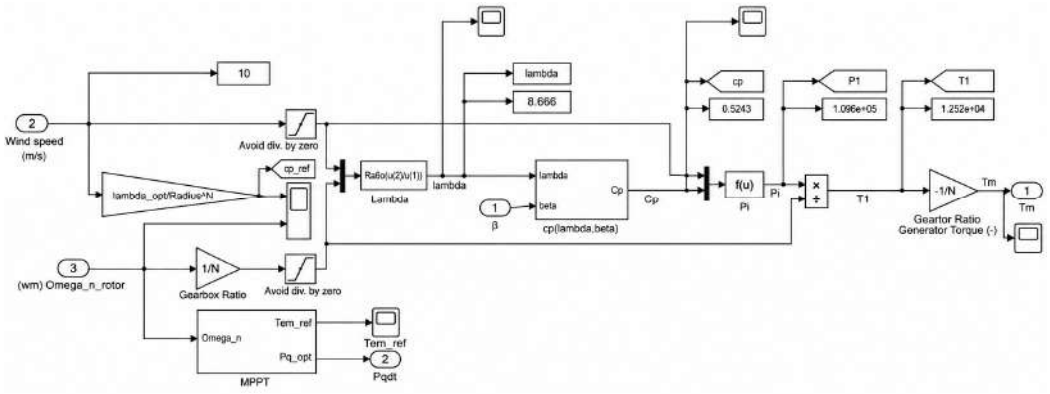


Figure 4. MATLAB/Simulink simulation model of the wind turbine aerodynamic and MPPT subsystem.

The turbine is connected to the generator through a gearbox with a speed ratio of:

$$i_g = \frac{\omega_m}{\omega_t} = 32 \tag{4}$$

where ω_m denotes the generator rotor speed and ω_t denotes the turbine angular speed. Therefore, the turbine angular speed is calculated as:

$$\omega_t = \frac{\omega_m}{i_g} = \frac{\omega_m}{32} \tag{5}$$

Accordingly, the mechanical power values presented in Table 1 are calculated using the turbine-side torque and angular speed as follows:

$$P = T_m \omega_t = \frac{T_m \omega_m}{i_g} = \frac{T_m \omega_m}{32} \tag{6}$$

Table 1. Turbine torque T_m, turbine angular speed ω_t, and mechanical output power P versus generator rotor speed ω_m at a wind speed of V = 10 m/s, assuming a gearbox ratio of i_g = 32.

ω_m, rad/s	0	8	16	32	64	128	157	256	350
ω_t, rad/s	0	0.25	0.5	1	2	4	4.906	8	10.938
T_m, N·m	0	0	0	95	6084	20200	19800	9728	1321
P, kW	0	0	0	0.095	12.168	80.8	97.144	77.824	14.448

An ideal gearbox with a mechanical efficiency of $\eta_g = 1$ is assumed; therefore, gearbox power losses are neglected. If gearbox losses are taken into account, the mechanical power on the generator side can be expressed as:

$$P_g = \eta_g T_m \omega_t \tag{7}$$

The results obtained from these calculations are summarized in Table 1 and plotted in Figure 5.

As shown in Figure 5, the maximum output power of approximately 97–100 kW is achieved when the generator rotor speed is close to 157 rad/s, which was therefore taken as the rated operating point of the generator for the rated wind speed of 10 m/s.

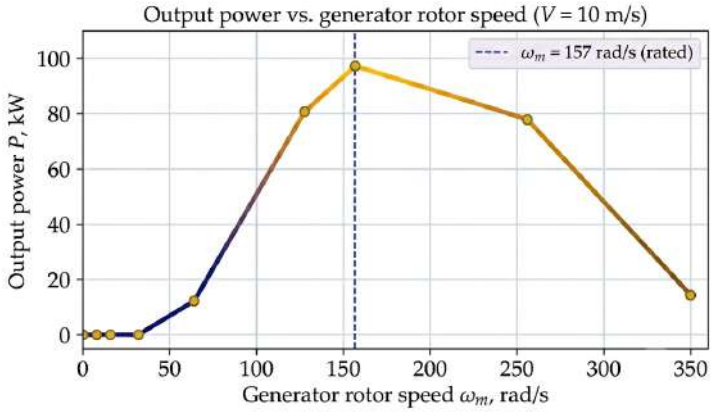


Figure 5. Output power of the wind energy conversion system as a function of the generator rotor speed at V = 10 m/s; the maximum power point is reached near ω_m = 157 rad/s.

2.3. Electromechanical Model of the Doubly Fed Induction Generator

The DFIG is a wound-rotor induction machine in which both the stator and rotor windings are connected to independent power sources: the stator winding is connected directly to the grid, while the rotor winding is fed through slip rings by the rotor-side converter, allowing the rotor current frequency, amplitude, and phase to be regulated so that the machine can generate power at both sub-synchronous and super-synchronous shaft speeds. Because the fundamental machine equations are nonlinear and time-varying in the stationary ABC reference frame, the model is transformed into the synchronously rotating dq0 reference frame using the Park transformation, which yields a linear, time-invariant representation suitable for vector control design. In the per-unit dq0 frame, the stator and rotor voltage equations are [10]:

$$\begin{cases} u_{ds} = -r_s i_{ds} - \frac{d\psi_{ds}}{dt} + \omega_s \psi_{qs} \\ u_{qs} = -r_s i_{qs} - \frac{d\psi_{qs}}{dt} + \omega_s \psi_{ds} \\ u_{dr} = r_r i_{dr} - \frac{d\psi_{dr}}{dt} - (\omega_s - \omega_r)\psi_{qr} \\ u_{qr} = r_r i_{qr} - \frac{d\psi_{qr}}{dt} - (\omega_s - \omega_r)\psi_{dr} \end{cases} \quad (8)$$

with the corresponding flux-linkage relationships:

$$\begin{cases} \psi_{ds} = L_s i_{ds} - L_m i_{dr} \\ \psi_{qs} = L_s i_{qs} - L_m i_{qr} \\ \psi_{dr} = -L_m i_{ds} - L_r i_{dr} \\ \psi_{qr} = -L_m i_{qs} - L_r i_{qr} \end{cases} \quad (9)$$

and the stator-side and rotor-side instantaneous active and reactive powers, neglecting losses, are obtained as:

$$\begin{cases} P_s = u_{ds} i_{ds} + u_{qs} i_{qs} \\ Q_s = u_{qs} i_{ds} - u_{ds} i_{qs} \\ P_r = u_{dr} i_{dr} + u_{qr} i_{qr} \\ Q_r = u_{qr} i_{dr} - u_{dr} i_{qr} \end{cases} \quad (10)$$

Because the stator winding is connected to a grid of essentially constant frequency and voltage, the stator resistance voltage drop can be neglected, and the stator-flux vector lags the stator-voltage vector by exactly 90°. This property is exploited in the stator-flux-oriented control scheme adopted in this work [6,10]: the d-axis of the rotating reference frame is aligned with the stator-flux vector, so that the q-axis component of the stator flux is identically zero (ψ_{qs} = 0), which decouples the active and reactive power channels

and allows them to be regulated independently through the rotor d- and q-axis current components, i_{dr} and i_{qr}, respectively.

2.4. Selected Machine and Turbine Parameters

The parameters used for the asynchronous (doubly fed) generator in the MATLAB/Simulink model were selected to satisfy a maximum output power of approximately 100 kW at the rated wind speed of 10 m/s and are summarized in Table 2.

Table 2. Parameters of the simulated wind turbine and Doubly Fed Induction Generator.

Parameter	Value
Rated power	100 kW
Rated stator voltage	380 V
Rated stator frequency	50 Hz
Stator resistance	0.26 Ω
Stator leakage inductance	0.3 mH
Rotor resistance	0.27 Ω
Rotor leakage inductance	0.3 mH
Mutual inductance	27.5 mH
Moment of inertia	0.2 kg·m^2
Minimum rotor radius (calculated)	11.08 m

2.5. Converter Topology and SVPWM

The rotor circuit and the grid are interconnected through a four-quadrant back-to-back AC/DC/AC converter, formed by two voltage-source inverters connected in anti-parallel through a common DC-link capacitor (Figure 6). This arrangement allows bidirectional active power flow: at sub-synchronous speed the rotor-side converter injects active power into the rotor circuit, whereas at super-synchronous speed, it extracts active power from the rotor circuit and feeds it back to the grid through the grid-side converter, while the DC-link capacitor decouples the two converter stages and suppresses harmonic interaction between them.

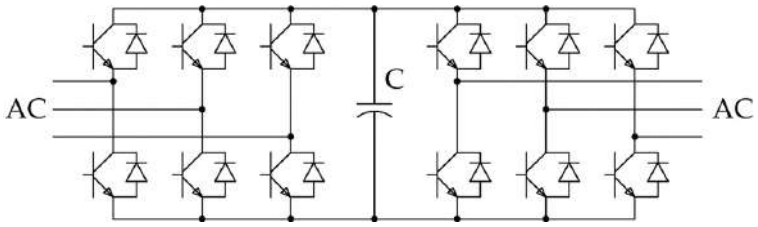


Figure 6. Structural diagram of the back-to-back four-quadrant voltage-source converter connecting the rotor circuit to the grid.

Each converter bridge is switched using space vector pulse-width modulation (SVPWM). In this technique, the eight possible switching states of a three-phase, two-level inverter (two zero vectors and six active vectors) divide the voltage plane into six 60° sectors; any reference voltage vector is synthesized as a time-weighted combination of the two adjacent active vectors bounding its sector, together with a zero vector, which is computed from the active sector number N and the corresponding vector application times T1 and T2. Compared with sinusoidal PWM, SVPWM provides a higher achievable DC-link utilization factor and lower harmonic distortion in the synthesized phase

voltages [11], both of which are beneficial for the dynamic performance of the rotor- and grid-side control loops.

2.6. Grid-Side Converter Control

The control objectives for the grid-side converter (GSC) are to (i) maintain a constant DC-link voltage with good dynamic response under varying rotor-side power flow [9], and ensure that the grid-side current is sinusoidal and in phase (or in a controlled phase relationship) with the grid voltage, so that the power factor at the point of common coupling remains close to unity. The grid-side converter topology used in the model is shown in Figure 7, where the AC side is connected to the grid through a series resistance-inductance filter and the DC side is connected to a smoothing/energy-storage capacitor.

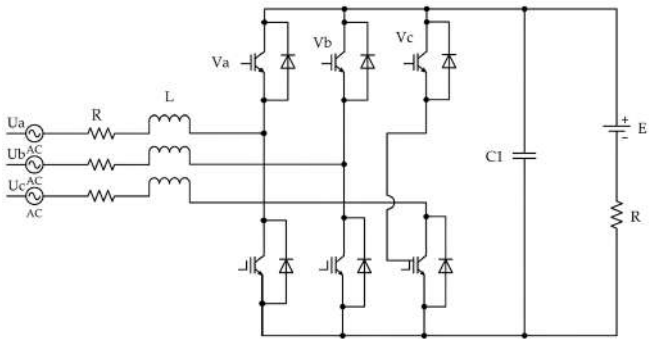


Figure 7. Topology of the grid-side PWM converter with R-L input filter and DC-link capacitor.

Grid-voltage-oriented vector control is applied to the grid-side converter: after the Park transformation, the d-axis of the rotating frame is aligned with the grid voltage vector, so that its q-axis component is zero. This yields the following relationship between the converter output voltage components and the d- and q-axis line currents:

$$\begin{cases} L\frac{di_{ds}}{dt} = -i_{ds}R + w_1 L i_{qs} + u_s - u_{ds} \\ L\frac{di_{qs}}{dt} = -i_{qs}R + w_1 L i_{ds} - u_{qs} \end{cases} \quad (11)$$

where u_{ds} and u_{qs} are the decoupling (cross-coupling compensation) terms. A dual closed-loop control structure is used: an outer DC-link voltage loop generates the active-current reference i_d^*, by comparing the measured DC-link voltage with its reference value through a PI controller, while an inner current loop regulates i_{ds} and i_{qs} to their references using PI controllers with feed-forward cross-coupling compensation. For unity power-factor operation, the reactive-current reference i_q^* is set to zero, so that the grid-side current vector remains in phase with the grid voltage vector. The resulting d- and q-axis voltage commands are transformed back to the three-phase frame and supplied to the SVPWM modulator, which generates the switching signals for the grid-side converter bridge.

2.7. Rotor-Side Converter Control

The rotor-side converter (RSC) implements stator-flux-oriented vector control [8]. With the d-axis aligned to the stator-flux vector ($\psi_{qs} = 0$) and stator resistance neglected, the stator active and reactive powers can be shown to be proportional to the q- and d-axis components of the rotor current, respectively, which allows the active and reactive power delivered through the stator to be controlled independently by regulating i_{qr} and i_{dr} [6]. To track the maximum power point of the turbine [14,15], the reference active power command is computed in real time from the optimal power–speed curve of the turbine for the measured rotor speed, and the corresponding rotor current references are generated and regulated through PI controllers, again with cross-coupling compensation between the d- and q-axis

loops. The reactive power reference is generally set to zero or to a value determined by grid voltage support requirements. The rotor-side converter, like the grid-side converter, uses the SVPWM scheme described in Section 2.5 to synthesize the required rotor excitation voltage at the slip frequency.

The complete MATLAB/Simulink representation of the DFIG electrical subsystem, including the stator and rotor measurement blocks, the machine model, and the AC sources representing the grid connection, is shown in Figure 8.

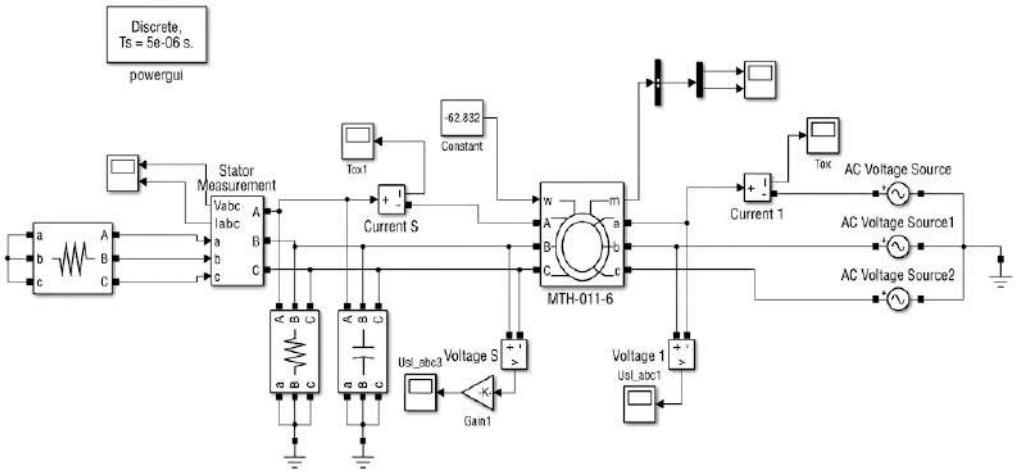


Figure 8. Model MATLAB/Simulink of a double-fed generator.

2.8. Simulation Setup

The complete system—wind turbine aerodynamic model, gearbox, DFIG electromechanical model, rotor-side converter with stator-flux-oriented vector control, grid-side converter with DC-link voltage control, and SVPWM modulators for both converters—was assembled and simulated in MATLAB/Simulink using a discrete solver with a fixed sample time of 5×10^{-6} s [13]. Simulations were performed for wind speeds of 5, 7, and 10.6 m/s in order to evaluate the system response in both the sub-synchronous and super-synchronous operating regions, and the active output power was additionally recorded over the continuous wind-speed range from 5 to 10.6 m/s to obtain the steady-state power–wind speed characteristic of the system. The principal performance criteria evaluated were (i) the settling time of the stator current following start-up, against the specified technical requirement of no more than 0.01 s, and (ii) the stabilization behavior of the DC-link voltage.

3. Result and Discussion

3.1. Generator Operation at Different Wind Speeds

The simulation model was first exercised at three representative wind speeds: 5 m/s and 7 m/s, at which the DFIG operates in the sub-synchronous regime, and 10.6 m/s, at which the generator operates in the super-synchronous regime. In all three cases, the overall three-phase output voltage settled to a stable sinusoidal waveform, while the output current displayed a pronounced but well-damped transient immediately after start-up, settling into a steady sinusoidal pattern within a few tens of milliseconds. The transient amplitude and the steady-state current magnitude both increased with wind speed, consistent with the higher mechanical power captured by the turbine and delivered to the grid through the stator and converter paths at higher wind speeds. The qualitative shape of the response—an oscillatory current transient with a duration on the order of 0.3–0.5 s before full settling to the periodic steady state, superimposed on an underlying fast initial current rise that settles within the first switching cycles—was repeatable across all three operating points, confirming that the stator-flux-oriented vector control loop maintains stable closed-loop

behavior across the full sub-synchronous to super-synchronous speed range required of the DFIG.

The stator current waveform during the initial start-up interval is of particular interest because it is governed by the specified technical requirement that the stator current must reach a steady state within 0.01 s. Figure 9 presents the characteristic shape of the stator current during the first 50 ms following start-up. The current exhibits an initial transient associated with the energization of the stator and rotor flux linkages and the initial response of the current control loop, after which it settles into a steady 50 Hz sinusoidal waveform. The settling behavior obtained from the model satisfies the 0.01 s technical requirement specified for the system, confirming that the bandwidth of the inner current control loop, combined with the cross-coupling compensation in the rotor-side and grid-side controllers, is sufficient to meet the prescribed transient-performance criterion.

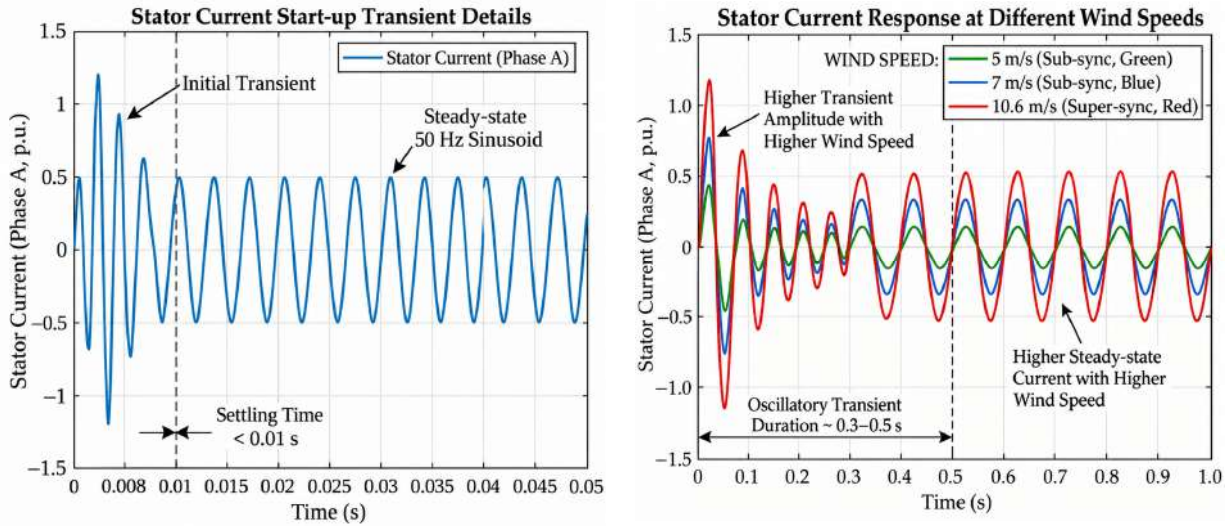


Figure 9. Simulation results for the DFIG. (**a**) Details of the stator current during the initial 50 ms start-up interval. The current settles into a steady sinusoidal waveform within 0.01 s, meeting the design requirement. (**b**) Stator current response for three representative wind speeds: 5 m/s, 7 m/s (sub-synchronous), and 10.6 m/s (super-synchronous). The graph shows that the transient magnitude and steady-state current increase with higher wind speeds, while maintaining stability across the full range.

3.2. Relationship Between Wind Speed and Output Power

The steady-state active output power of the system was evaluated as a function of wind speed over the range from 5 m/s to 10.6 m/s, with the results presented in Figure 10. As expected from the cubic dependence of available aerodynamic power on wind speed (Equation (1)), the output power increases monotonically and with an increasing slope as the wind speed rises, reaching the rated value of approximately 100 kW at the rated wind speed of 10.6 m/s. At the lower end of the tested range (5 m/s), the output power is approximately 10–11 kW, reflecting the cubic power–wind speed relationship together with the power coefficient achieved by the maximum power point tracking algorithm at that operating point.

This characteristic confirms that the maximum power point tracking strategy embedded in the wind turbine and rotor-side converter control successfully follows the optimal power curve defined by $C_{p.max}$ and λ_{opt} (Section 2.2) across the operating wind-speed range, allowing the system to extract close to the maximum available aerodynamic power at each wind speed while remaining within the rated capacity of the generator and converter.

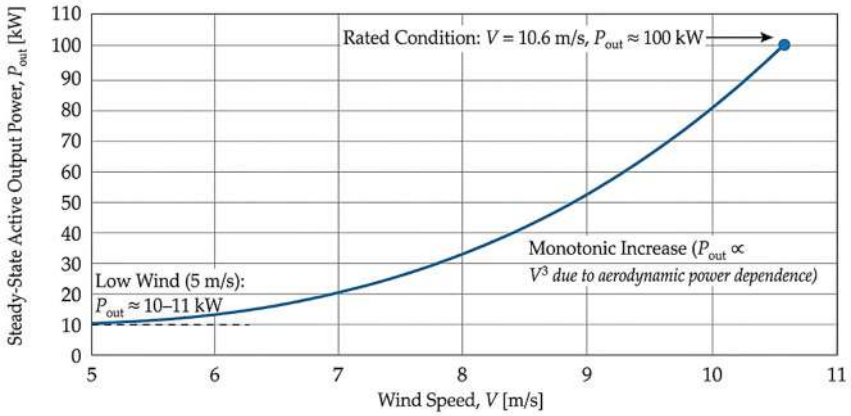


Figure 10. Relationship between the total active output power P (kW) and wind speed V (m/s) obtained from the simulation.

3.3. DC-Link Voltage Stabilization

The behavior of the DC-link voltage during system start-up and steady-state operation is shown in Figure 11. Upon energization, the DC-link capacitor exhibits an oscillatory charging transient, with the voltage initially overshooting and undershooting around the reference value before the oscillations are progressively damped by the grid-side converter's voltage control loop. After approximately 0.5 s, the DC-link voltage settles to a stable value of approximately 700 V, which corresponds to the reference value set for the DC-link voltage controller and confirms that the grid-side converter maintains the energy balance between the rotor-side and grid-side converter stages under the simulated operating conditions.

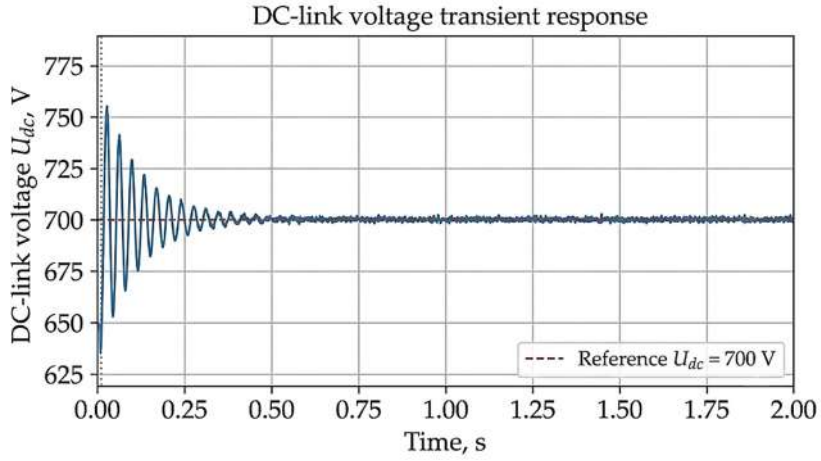


Figure 11. Simulated DC-link voltage waveform; the voltage stabilizes at approximately 700 V after an initial damped oscillatory transient of about 0.5 s.

The stability of the DC-link voltage is critical for reliable converter operation, since excessive voltage ripple or sustained oscillations could lead to increased switching stress on the power semiconductor devices and degraded power quality on both the rotor and grid sides. The damped, well-behaved settling pattern observed in Figure 11 indicates that the outer DC-link voltage loop of the grid-side converter [9], in combination with the inner current loop, provides adequate damping and bandwidth for the chosen DC-link capacitance and controller gains used in the model.

3.4. Discussion

The combination of stator-flux-oriented vector control on the rotor side, grid-voltage-oriented vector control on the grid side, and SVPWM for both converter stages was found to

provide effective decoupling between the active and reactive power channels, allowing the active power reference—derived from the maximum power point tracking algorithm—to be tracked independently of the reactive power setting. This decoupled structure is the principal mechanism by which the system achieves both the rapid stator current settling time (Section 3.1) and the stable DC-link voltage regulation (Section 3.3) simultaneously, since perturbations in one power channel do not propagate into the other under the cross-coupling-compensated control scheme described in Sections 2.6 and 2.7.

Compared with a hypothetical scalar (non-vector) control approach, in which active and reactive power cannot be regulated independently and transient response is generally slower and less damped, the vector control approach adopted in this study achieves markedly improved dynamic characteristics, evidenced by the sub-0.01 s stator current settling time and the well-damped DC-link voltage transient. These results are consistent with reported advantages of stator-flux-oriented and grid-voltage-oriented vector control schemes in the wind energy literature [6,10], and they further support the suitability of the DFIG configuration, with its partial-scale back-to-back converter, for small-scale wind energy systems intended for operation alongside an external power supply system in a microgrid context.

From a system-level perspective, the results also confirm that the modeled wind energy conversion system can operate stably within a microgrid environment: the stator remains directly and continuously connected to the external supply system throughout all simulated wind-speed transitions, while the converter-mediated rotor circuit absorbs the variability introduced by fluctuating wind speed without producing unacceptable disturbances on the grid side, in terms of either current transients or DC-link voltage excursions. This is consistent with the functional-safety perspective discussed for the broader system design, in which the coordinated, well-damped behavior of the control loops reduces the likelihood of safety-relevant failure modes associated with control-system malfunction or parameter mismatch during variable-wind-speed operation [12].

Certain limitations of the present study should be acknowledged. The simulation results were obtained for discrete wind-speed operating points and for a fixed-parameter linear PI-based control structure; further work could extend the analysis to continuously varying (stochastic) wind-speed profiles, to grid-fault scenarios for verifying fault ride-through capability, and to comparative evaluation against alternative control strategies such as direct power control or model predictive control, which have been proposed in the literature as a means of further improving the dynamic response and robustness of DFIG-based wind energy conversion systems.

4. Conclusions

This study presented the development and MATLAB/Simulink-based verification of a complete model of a wind energy conversion system based on a Doubly Fed Induction Generator operating in conjunction with an external power supply system. The model integrated an aerodynamic wind turbine subsystem with maximum power point tracking, an electromechanical DFIG subsystem represented in the synchronously rotating dq0 reference frame, and a back-to-back AC/DC/AC converter controlled through stator-flux-oriented vector control on the rotor side and grid-voltage-oriented vector control on the grid side, with both converter stages modulated using space vector pulse-width modulation.

The simulation results showed that the rotor radius required to deliver a rated output of 100 kW at a wind speed of 10 m/s is approximately 11.08 m, and that the corresponding rated generator rotor speed is approximately 157 rad/s. The active output power of the system increased monotonically with wind speed over the tested range of 5–10.6 m/s, reaching the rated 100 kW value at the rated wind speed, consistent with the maximum

power point tracking strategy implemented in the turbine and rotor-side converter control. The stator current was shown to settle to its steady-state sinusoidal waveform within the specified technical requirement of 0.01 s, confirming the adequacy of the inner current control loop bandwidth. The DC-link voltage was shown to stabilize at the design value of approximately 700 V following a damped oscillatory transient of about 0.5 s, confirming the effectiveness of the grid-side converter's voltage control loop.

These results demonstrate that the combined stator-flux-oriented and grid-voltage-oriented vector control strategy, implemented together with SVPWM, provides an effective and robust approach for the modeling and control of small-scale DFIG-based wind energy conversion systems intended for stable operation alongside an external power supply system, including microgrid applications in which frequency and voltage stability are particularly sensitive to the variability of renewable generation. Future work will extend the present model to continuously varying stochastic wind-speed profiles, grid-fault and fault ride-through scenarios, and comparative evaluation against alternative nonlinear and predictive control strategies, in order to further assess and improve the robustness of the proposed control approach under a wider range of operating conditions.

Author Contributions: Conceptualization, S.S. and S.D.; methodology, S.S.; software, S.S.; validation, S.D., J.K., K.Y. and G.M.; formal analysis, S.S.; investigation, S.S.; resources, S.S.; data curation, S.S.; writing—original draft preparation, S.S.; writing—review and editing, S.D.; visualization, S.S.; supervision, S.S.; project administration, S.S. All authors have read and agreed to the published version of the manuscript.

Funding: This research received no external funding.

Institutional Review Board Statement: Not applicable.

Informed Consent Statement: Not applicable.

Data Availability Statement: The data presented in this study are available on request from the corresponding author.

Conflicts of Interest: The authors declare no conflicts of interest.

References

1. BP. *BP Statistical Review of World Energy 2019*; BP plc: London, UK, 2019. Available online: https://www.bp.com/en/global/corporate/energy-economics/statistical-review-of-world-energy.html (accessed on 1 September 2026).
2. National Energy Administration. Transcript of the National Energy Administration Online Press Conference, First Quarter of 2021. 2021. Available online: http://www.nea.gov.cn/2021-01/30/c_139708580.htm (accessed on 1 September 2026).
3. State Council Information Office of the People's Republic of China. *China's Energy Development in the New Era*; State Council Information Office: Beijing, China, 2020.
4. Liu, C.; Huang, Y.; Zhang, N.; Li, X.; Liu, D.; Yao, J. Renewable energy dispatching based on smart grid dispatching and control system platform. *Autom. Electr. Power Syst.* **2015**, *39*, 159–163. [CrossRef]
5. Chhipa, A.A.; Chakrabarti, P.; Bolshev, V.; Chakrabarti, T.; Samarin, G.; Vasilyev, A.N.; Ghosh, S.; Kudryavtsev, A. Modeling and control strategy of wind energy conversion system with grid-connected doubly-fed induction generator. *Energies* **2022**, *15*, 6694. [CrossRef]
6. Idrissi, I.; Chafouk, H.; El Bachtiri, R.; Khanfara, M. Modeling and simulation of the variable-speed wind turbine based on a doubly fed induction generator. In *Gas Turbines—Control, Diagnostics, Simulation, and Measurements*; IntechOpen: London, UK, 2019. [CrossRef]
7. Aljafari, B.; Stephenraj, J.P.; Vairavasundaram, I.; Rassiah, R.S. Steady-state modeling and performance analysis of a wind turbine-based doubly fed induction generator system with rotor control. *Energies* **2022**, *15*, 3327. [CrossRef]
8. Bouazza, F.; Mohamed, M.; Abdelhamid, L.; Mohamed, L.K. Control of grid-connected PMSG-based wind turbine system with back-to-back converter topology using resonant controller. *Int. J. Mech. Ind. Aerosp. Sci.* **2020**, *14*, 201–207.
9. Nian, H.; Xu, Y.; Chen, L.; Zhu, M. Modeling and analysis of DC-link dynamics in DFIG system with an indicator function. *IEEE Access* **2019**, *7*, 125401–125412. [CrossRef]

10. Prasad, R.M.; Mulla, M.A. Mathematical modeling and position-sensorless algorithm for stator-side field-oriented control of rotor-tied DFIG in rotor flux reference frame. *IEEE Trans. Energy Convers.* **2020**, *35*, 631–639. [CrossRef]
11. Alwash, S.M.; Al-Thahab, O.Q.J.; Alwash, S.F. Modeling and control strategies for DFIG in wind turbines: A comparative analysis of SPWM, THIPWM, and SVPWM techniques. *J. Eur. Syst. Autom.* **2023**, *56*, 963–972. [CrossRef]
12. Talani, R.A.; Kaloi, G.S.; Ali, A.; Bijarani, M.A.; Abbas, G.; Hatatah, M.; Mercorelli, P.; Touti, E. Dynamic performance analysis and fault ride-through enhancement by a modified fault current protection scheme of a grid-connected doubly fed induction generator. *Machines* **2025**, *13*, 110. [CrossRef]
13. Rajendran, M.; Kumar, L.A. Modeling and simulation of a DFIG-based wind energy system. In *Advances in Smart Grid Technology*; Siano, P., Jamuna, K., Eds.; Lecture Notes in Electrical Engineering; Springer: Singapore, 2020; Volume 687, pp. 31–49. [CrossRef]
14. Chhipa, A.A.; Vyas, S.; Kumar, V.; Joshi, R.R. MPPT optimisation techniques and power electronics for renewable energy systems: Wind and solar energy systems. *Int. J. Swarm Intell.* **2022**, *7*, 141–167. [CrossRef]
15. Mousa, H.H.; Youssef, A.R.; Mohamed, E.E. Variable step-size P&O MPPT algorithm for optimal power extraction of a multiphase PMSG-based wind generation system. *Int. J. Electr. Power Energy Syst.* **2019**, *108*, 218–231. [CrossRef]

Disclaimer/Publisher's Note: The statements, opinions and data contained in all publications are solely those of the individual author(s) and contributor(s) and not of MDPI and/or the editor(s). MDPI and/or the editor(s) disclaim responsibility for any injury to people or property resulting from any ideas, methods, instructions or products referred to in the content.